BIOMIMICRY OF NATURAL REEF HYDRODYNAMICS IN AN ARTIFICIAL SPUR AND GROOVE REEF FORMATION

Emilee Wissmach[1], Matthew Ninesling[1], and Robert J. Weaver[1]

An artificial spur-and-groove (SAG) reef formation designed to perform as a submerged breakwater was studied. Not only do natural SAG reefs effectively attenuate waves, but they also create important circulation within the system that encourages the success of corals and the overall ecosystem. Modular components were developed and imported into the CFD software FLOW-3D® HYDRO to test the wave-structure interaction while adjusting the geometry of the structure, wave conditions, and depth due to tidal changes in environmental conditions similar to Moloka'i, Hawaii. Results showed highest wave height reduction with larger wave heights as well as lower submergence during low tide conditions.

Keywords: spur and groove reefs; FLOW-3D® HYDRO; artificial reef; submerged breakwater; numerical modelling; green engineering

INTRODUCTION

Shorelines around the world are increasingly at risk from sea level rise as a result of climate change. Not only are sea levels encroaching more into the coast, but storms are also becoming more frequent and severe with larger waves that will have a greater impact on a shoreline's morphology (Masselink et al. 2016; Vousdoukas et al. 2020). Given that 41% of the world population lives on the coast, there is high demand to protect the property and homes in these areas (Martínez et al. 2007). Typical structures used to mitigate coastal erosion include groins, seawalls, and emergent breakwaters which are costly and disrupt the natural setting (United States 2006). Submerged breakwaters, however, do not disrupt the aesthetics of the beach, allow for normal cross-shore sediment processes to occur with smaller waves, and facilitate ideal water quality in the lee of the structure (Irtem et al. 2011; Kobayashi & Wurjanto 1989). As wave height increases, there is more interaction between the structure and the bottom of the wave, which is crucial for their role in attenuating storm waves. Extensive research and development of equations to ensure stability and proper design of breakwaters has been done in the past hundred years; however, nature has long before established coral reefs as effective natural breakwaters worldwide given the existence of ancient SAG morphology dating back to the mid-Paleozoic period, over 350 million years ago (Campos et al. 2020; Duce et al. 2016; Wood & Oppenheimer 2000).

Amongst the different type of reef formations, spur-and-groove reefs are specifically noted for their ability to act as natural breakwaters that regulate hydrodynamic energy and promote optimal nutrient flows to encourage life on the reef platforms (Duce et al. 2014; Munk & Sargent 1948).

Figure 1. SAG reef formation on Sombrero Key from Google Maps.

[1] OEMS Department, Florida Institute of Technology, 150 W University Blvd, Melbourne, FL, 32901, United States

The overall structure is composed of multiple large ridges (spurs) separated by sections of sediment floor (grooves) that start after the reef flat near the shoreline and extend into deeper water down the reef slope (da Silva et al. 2020). A typical SAG reef at Sombrero Key in the Florida Keys is shown in Figure 1.

The geometry of SAG zones has been well documented, but not until recently have the hydrodynamics been 3D modeled and studied more thoroughly by da Silva et al. (2020). Researchers have found that the SAG geometry is correlated to the incident wave conditions and that different geometric traits affect the hydrodynamics and circulation within the reef system (Acevedo-Ramirez et al. 2021; da Silva et al. 2020; Duce et al. 2016; Rogers et al. 2013). The geometry of the structures considers an array of parameters including spur height, spur length, spur wavelength, groove width, cross-shore slope, and the reef flat width (da Silva et al. 2020; Duce et al. 2016). Duce et al. (2016) notes that numerous authors describing SAG reefs in their work use different terminology and metrics, making comparison of data and general understanding of differences between reefs difficult. Therefore, the terminology from Duce et al. (2016) was adopted for use here.

Global coral reef populations have been declining all around the world, with recent studies stating that current living reef coverage has declined by 50% since the 1950s. These ecosystems provide food, job opportunities, carbon sequestration, and coastline protection from extreme climate events (Eddy et al. 2021). While numerous entities have aimed to create artificial reefs to promote life, few have integrated wave attenuation properties into the design for coastline protection. Similarly, not all coastline protection structures provide the complex habitats that the natural environment does (Gittman et al. 2016).

A living coral reef breakwater that mimics SAG reef tracts could protect vulnerable coastlines while also adding an essential ecosystem. Additionally, these reefs are able to readily adapt to local conditions to reduce long-term maintenance costs (FIO 2021). Not only will the corals grow in a way tuned to the wave conditions, but they will also grow vertically and laterally creating more complex surface area while adjusting for sea level rise. Encrusting coralline red algae builds up reefs via internal marine precipitation of aragonite and magnesium calcite, and this process is expedited based on the influx of new seawater (Banks et al. 2007). When extreme weather events happen and some corals are damaged, the living breakwater will have the ability to self-heal. This integrated and diverse ecosystem approach could exceed the design life of other man-made structures, create a hotspot for fishing and tourism, and rehabilitate an ecosystem type that is rapidly dwindling.

MATERIALS AND METHODS

Design and Mesh Development

The design idea behind the structures of the reef stemmed from the Consortium for Advanced Reef Restoration Engineering and Technologies (CARRET) proposal created by FIO, Figure 2a. The total structure consists of three different parts including: berms in the groove area that encourage wave-shoaling and mitigate scouring, spurs that initiate wave breaking and circulation, and crests behind the spurs to dissipate any remaining wave energy (FIO 2021).
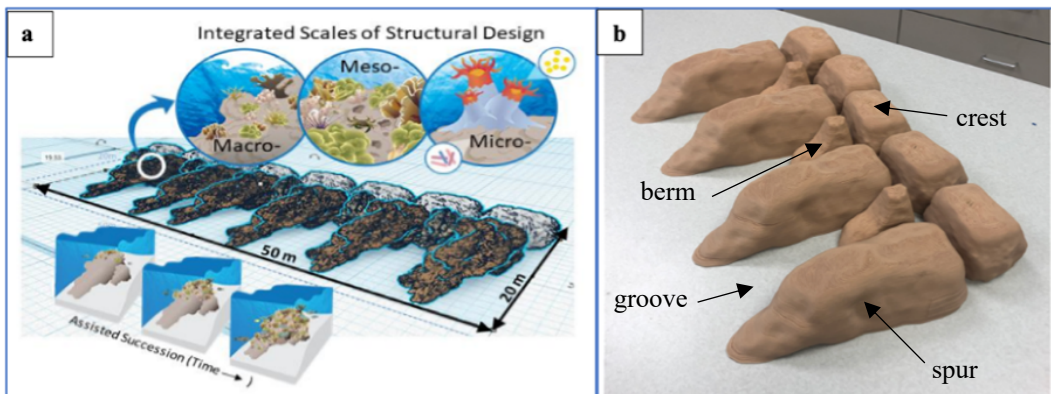

Figure 2. Conceptual designs inspired from typical SAG reefs in nature that were adjusted to correlate to a novel submerged breakwater/artificial reef design. a. Schematic of proposed SAG design from CARRET proposal b. 3D printed modules inspired from CARRET proposal.

The literature shows that the SAG zones and the reef crest/flat zones contribute to wave dissipation under varying conditions, so it was important to include both aspects in the design. Duce et al. (2022) observed that the SAG zones dissipate more wave energy under higher wave conditions at low tide, and the reef crest/flat zone dissipates more wave energy during high tides and smaller wave conditions. Since the goal is to attenuate larger waves that are more erosive, the bulk of the volume of the structure was allocated to the spurs.

To get 3D meshes of each module, coquina rock was carved to resemble the berm, spur, and crest. Photogrammetry methods were used through the Foldio360 iPhone app and a turn table. After the 3D images were obtained, they were uploaded to Agisoft where the mesh was created. Meshmixer was used to repair any holes or errors in the mesh and scale the modules to an appropriate size. Files were then converted to the sliced G-Code format in Slic3r, and modules were 3D printed, Figure 2b.

Preliminary Work

A detailed literature review was done to quantify typical dimensions for SAG reefs in nature. One project goal was to test the sensitivity of wave response to these dimensions and determine which are the most important parameters to focus on for design optimization. While there are numerous variables involved, ones that were considered the most influential on the flow were chosen to keep the work within the scope of this project. Spur length, crest length, groove width, incident wave height, wave period, and a set depth under varying tidal conditions were chosen to vary in the sensitivity tests, with length defined here in the cross-shore direction. While spur height and spur width are parameters that would still potentially affect the flow, they were decided to remain constant to reduce the overall number of variables.

SAG reefs vary greatly worldwide, with ranges of dimensions provided in Table 1. For this research these ranges were narrowed down by considering feasibility of construction of a submerged breakwater. Duce et al. (2016) analyzed a significant amount of SAG reefs and was able to separate them into four different categories: Class 1 – Deep and disconnected (DaD), Class 2 – Exposed to wave energy (EWE), Class 3 – Long and protected (LaP), and Class 4 – Short and protected (SaP). Since the purpose of the artificial reef modules is to attenuate wave energy at the coast, the design should mimic the Class 2 SAG reefs; therefore, the data ranges from this study were specifically chosen for that class.

Table 1. Range of SAG dimensions from literature review.			
Type	Source	Range of Values	Unit
Wave height	Rogers et al., 2013	0.25-2.5 (H_i)	m
	da Silva et al., 2020	0.5-6.0 (H_s)	m
Wave period	Rogers et al., 2013	8-22	s
	da Silva et al., 2020	3-15	s
Spur length	Duce et al., 2016	1.5-654	m
Groove width	Duce et al., 2016	1-2[a]	m
	da Silva et al., 2020	0.25-82	m
	Rogers et al., 2013	0-196.8	m
	Blanchon & Jones, 1995	<3[a]	m
Depth	Blanchon & Jones, 1995	5-15[a]	m
	Duce et al., 2016	5-8[b]	m
Spur height	da Silva et al., 2020	0.5-8.0	m
	Rogers et al., 2013	0-8.0	m
	Duce et al., 2016	1.0-2.5[a]	m
Spur width	Duce et al., 2016	5-23[a]	m
Bed slope	Rogers et al., 2013	7% (fore reef) in depths 3-30 m	-
	Duce et al., 2016	2.3[oa]	-

[a]Ranges only from Class 2 – Exposed to wave energy (EWE) category that Duce et al. (2016) reported.
[b]This range includes average depths on different reefs in the high wave exposure class.

All parameters above were clearly comparable and executable for the spur and grooves; however, the crest and berm modules were not. Reef crests, the transitional area located at the beginning of the reef flat or the back reef lagoon, were not found to be specifically quantified in the literature review and were grouped together with the reef flat for total area in Duce et al. (2022). As seen in Figure 3, the reef flat area is exponentially larger than the proposed "crest" module of the artificial reef.
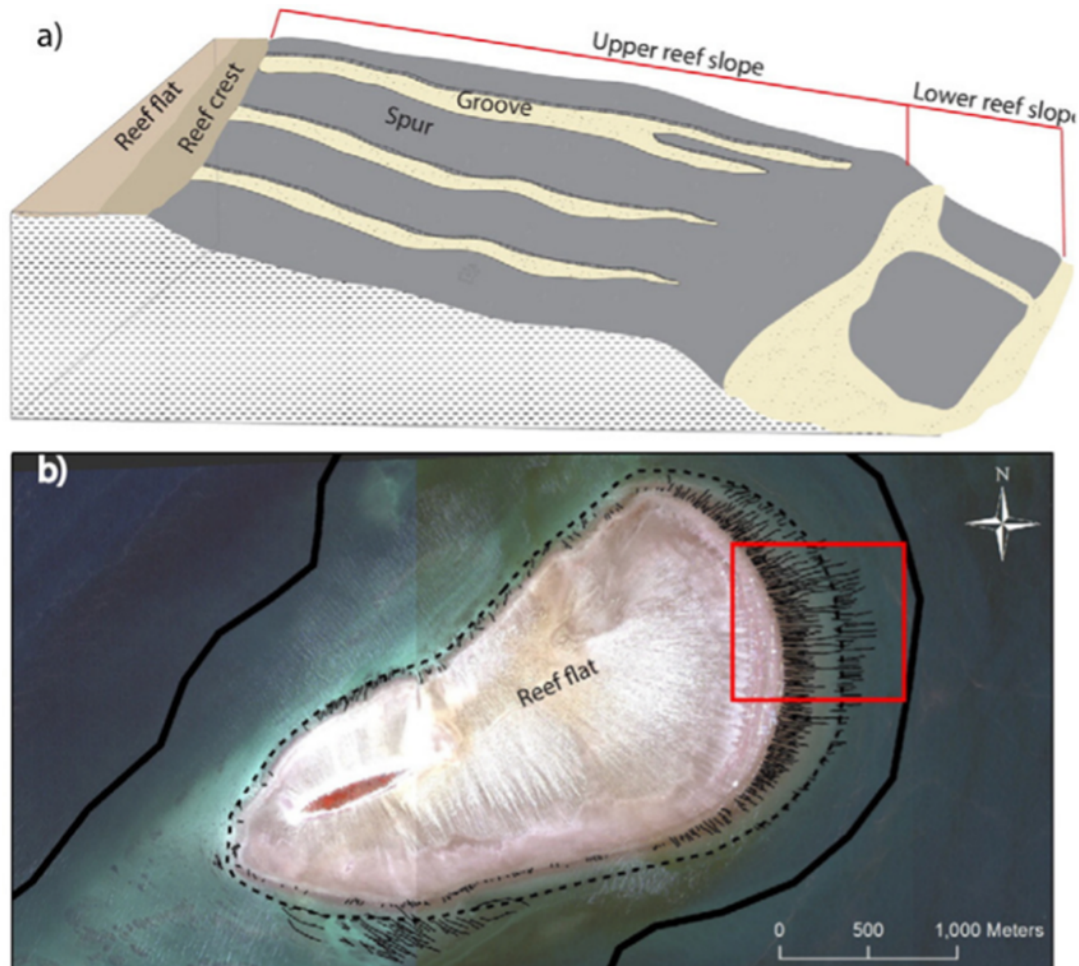
Figure 3. Schematic from Duce et al. (2016) showing a typical SAG reef formation. a. Graphic showing spurs (ridges of corals) and grooves (sandy bottom areas adjacent to the spurs) that are in the upper reef slope and are followed by the reef crest and reef flat. b. Aerial image elucidating the size comparison between the upper reef slope and the reef flat on Wreck Reef in the Southern Great Barrier Reef.

Clearly this part of the reef cannot be on the same scale as the artificial spur and grooves; therefore, the crest module's dimensions were arbitrarily chosen, and it was noted that more extensive testing would likely need to focus on this part of the reef since its function needs to assume the role of the reef crest/flat zone. Since the crest module was potentially going to be in the breaker zone as well, the dimensions here needed to consider the potential effects on the currents and scour behind the structure. The berm module is similar in that it is not an evident part of a natural SAG reef, but it was added to prevent scouring at the toe of the crest modules as its main function. Given that purpose, the berm was set to adjust accordingly based on changes in groove width.

To test the influence of each module on the hydrodynamics of the system as well as the wave attenuation, sensitivity tests were run similar to the process shown in da Silva et al. (2020). An initial case scenario was chosen based on the previous values found in the literature, while remaining within feasible dimensions of a conventional rubble mound breakwater, Table 2.

Table 2. Base case scenario that was used during the sensitivity runs which consisted of keeping these input parameters the same while individually varying one parameter at a time.			
Boundary	Base Case	Range	Unit
Spur Width	5	-	m
Roughness Height	0.14	-	m
Spur Height	4.8	-	m
Bed Slope	5%	-	-
Depth	6	5.1-6.9	m
Wave Height	2	0.5-4	m
Wave Period	10	6-15	s
Groove Width	2	1-4	m
Spur Length	30	20-60	m
Crest Length	8	4-12	m

The depth at the end of the spur and the beginning of the crest was chosen to be 6 m, based on similar values in the literature, and the spur height was chosen to be 4.8 m, based on tidal conditions in Moloka'i Hawaii which was the reference reef modeled in da Silva et al. (2020) (Duce et al. 2016; Ogston et al. 2004; Storlazzi et al. 2004). From an engineering perspective the low submergence height was also selected because submerged breakwaters with a smaller crest submergence value have a lower transmission coefficient (Dattatri et al. 1978). Additionally, the spur width remained constant at 5 m to reduce the number of variables changed and was concluded to not be a main contributor to the hydrodynamics. Lastly, a roughness height of 0.14 m was implemented on the spurs to simulate the roughness of corals as used by Lowe et al. (2009) and Rogers et al. (2013).

CFD Program

To perform the CFD analysis, an educational license for FLOW-3D® HYDRO was requested and permitted for use. Once installed, the stereolithography meshes were imported into the software. The modules were scaled to reasonable dimensions that aligned with the literature, and test simulations were run. FLOW-3D® HYDRO is a valuable tool for this problem since the program uses the FAVOR™ (Fractional Area/Volume Obstacle Representation) method. This approach is well suited for complex geometries since it defines the mesh with fractional face areas and volumes providing accurate outlines of the mesh rather than rigid cell block outlines of the structure (Flow Science, Inc. 2008).

The simulation was set up with two spurs, one berm in between the spurs, and two crests behind the modules. Multiple probes were placed in the mesh at the deep-water limit of the sloped bed, approximately 10 m in front of the structure, above the spur and groove, on the groove floor, and at a minimum half a wavelength behind the structure to record data. To decrease computation time and file size, a variable mesh was used starting at 1 m at the x-minimum and x-maximum boundaries then transitioning to 0.2 m closer to the structure. The boundary conditions for the mesh block are provided in Table 3.

Table 3. Boundary conditions for the mesh in FLOW-3D® HYDRO.	
Boundary	Type
X Minimum (Forced Inflow Boundary)	Stokes and Cnoidal Wave
X Maximum (Outflow Boundary)	Wave Outflow
Y Minimum (Wall Boundary)	Symmetry
Y Maximum (Wall Boundary)	Symmetry
Z Minimum (Bottom Boundary)	Symmetry
Z Maximum (Upper Boundary)	Pressure

Stokes and Cnoidal (Fourier series method) waves were set to propagate from the inflow boundary towards the outflow boundary, where an additional dampening region was added to minimize wave

reflection. All symmetry values inform the program to employ a free-slip condition to ensure the normal component of the fluid velocity is equal to zero at that boundary. The RNG turbulence model was used which dynamically computes the turbulent mixing length for RANS models (Yakhot & Orszag 1986). Given the mesh size and parameters provided, the software adjusts the time-step based on stability and convergence throughout the entirety of the simulation. Final setup based on conditions from Moloka'i, Hawaii is shown below.
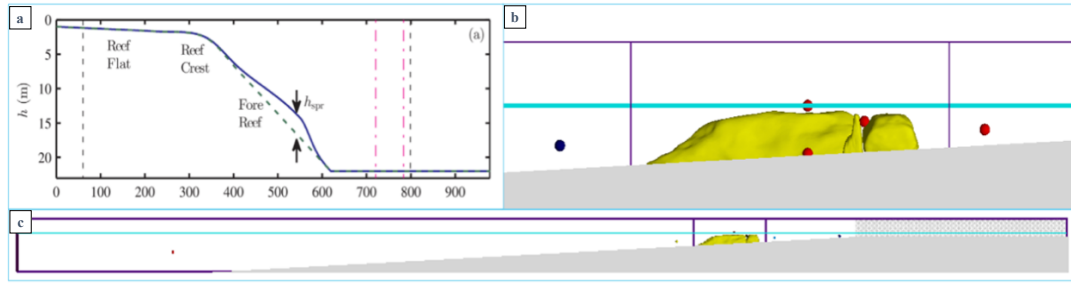
Figure 4. Visualization of domain setup for the simulations in this study compared to the setup in da Silva et al. (2020). a. da Silva et al. (2020) physical dimensions based on the reef in Moloka'i, Hawaii b. FLOW-3D® HYDRO arrangement of SAG model (yellow) on sloping bed (grey) with SWL depicted by the blue horizontal line. Probe locations in the groove and adjacent to structure are indicated by blue and red dots. c. The entire model domain for simulation in FLOW-3D® HYDRO with SAG model in yellow, SWL in blue, and sloping bed in grey with probe locations indicated by the dots.

Analysis Methods

The hydrodynamics of the artificial SAG system were studied in response to varying wave conditions, tidal ranges, and morphology. Wave height reduction, the transmission coefficient, turbulent dissipation within the groove and above the spur, velocity profiles, breaking location, and other flow patterns were all studied. Since FLOW-3D® HYDRO provides free surface elevation at probes, the data was exported into MATLAB to find wave height by detrending the free surface elevation data using the zero up crossing method. The wave height reduction calculation utilized the wave height approximately 10 m before the structure and the wave height at a minimum of half a wavelength after the structure and was calculated with the given equation:

$$H(\%) = \frac{H_1 - H_2}{H_1} * 100 \qquad (1)$$

Transmission coefficient was additionally calculated with the equation given by:

$$C_t = \frac{H_2}{H_1} \qquad (2)$$

For further analysis FLOW-3D®'s post processing software, FLOW-3D® POST, was used providing powerful visualization of wave breaking and wave-structure interactions. Turbulent dissipation along with the breaking location were main indicators to the locations where most of the wave energy was being attenuated. Velocity profiles additionally indicated direction and magnitude of flow.

RESULTS

The initial case scenario was first studied to understand how the flows behaved in the control conditions, and then the results of changing the parameters during the sensitivity runs were analyzed. The most significant change that occurred was when the wave height increased. As wave height increased, the breaking location occurred earlier on the structure, and the velocity and turbulent dissipation increased. There was no breaking in the H = 0.5 m case, Figure 5a. With an increased wave height of 2 m, the wave broke on the crest module, Figure 5b. At the largest tested wave height, H = 4

m, breaking occurred just in front of the crest module, Figure 5c. A turbulent cell within the groove was also notable in the 4 m wave height condition.
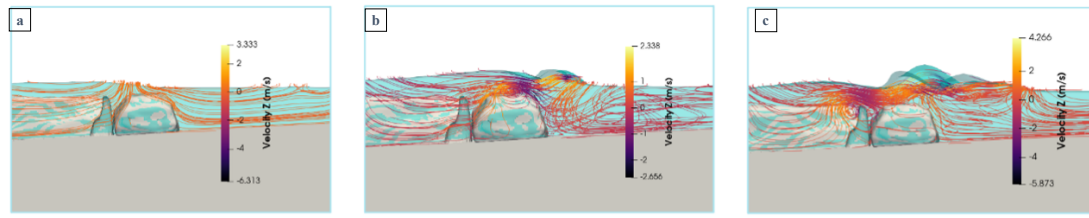
Figure 5. Wave breaking locations and z-velocity streamlines under varying wave heights with constant wave period of T = 10 s. a. H = 0.5 m wave condition where no wave breaking occurred on the structure and minimal z-velocities were observed. b. H = 2 m wave condition where wave breaking occurred on the crest module and negative z-velocities were observed. c. H = 4 m wave condition where wave breaking occurred before the crest module and negative z-velocities were observed.

With the largest wave, return flows after wave breaking were noted to be coming through the groove from the lee of the structure to meet the incoming wave. The smaller wave saw an insignificant amount of turbulence and did not break over the structure. Increasing intensity of turbulence and wave breaking correlated to higher wave height reduction trends, Figure 6.
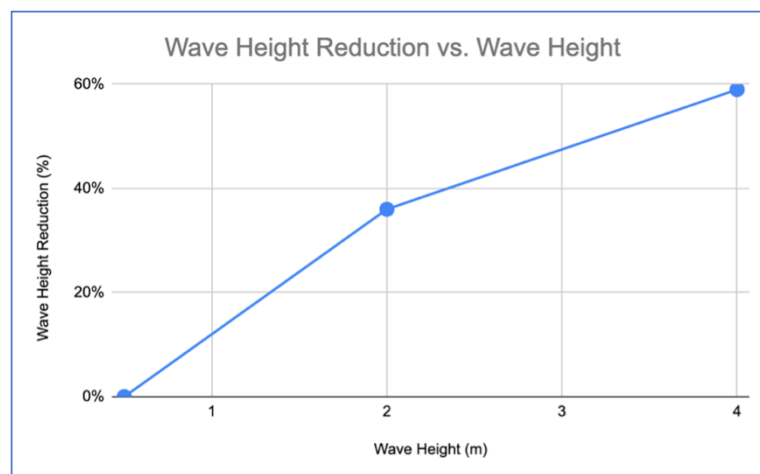
Figure 6. Plot showing significant increase in wave height reduction as wave height increases which is likely attributed to the larger wave heights having more energy to be dissipated. Note that wave height reduction here includes wave shoaling; therefore, dissipation is not fully attributed to the structure.
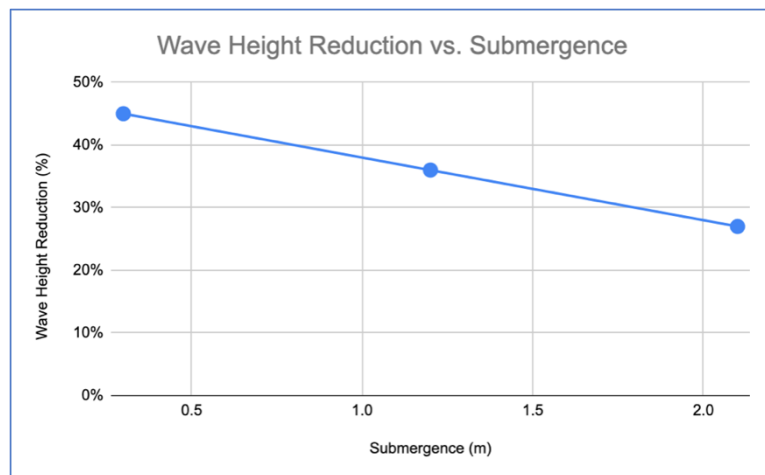
As wave height increased, wave height reduction significantly increased likely due to the greater amount of energy that could be attenuated and increased interaction with the structure.

Submergence levels, the distance between the top of the structure and the water level, were tested as well, and results showed much higher wave height reduction and increased turbulent dissipation in the lower tide condition (i.e. smallest submergence) compared to the high tide condition (i.e. largest submergence). Testing the low tide condition, Figure 7a, indicated that the wave breaks (upper image) on the structure and resulted in increased turbulent dissipation levels (lower image) in the berm area (probe in between the berm and crest module) as well as on the spur surface. These observations contrasted with the high tide condition, Figure 7b, where the wave begins to steepen but has not yet broken (upper image) which likely contributed to the negligible amount of turbulent dissipation recorded (lower image).
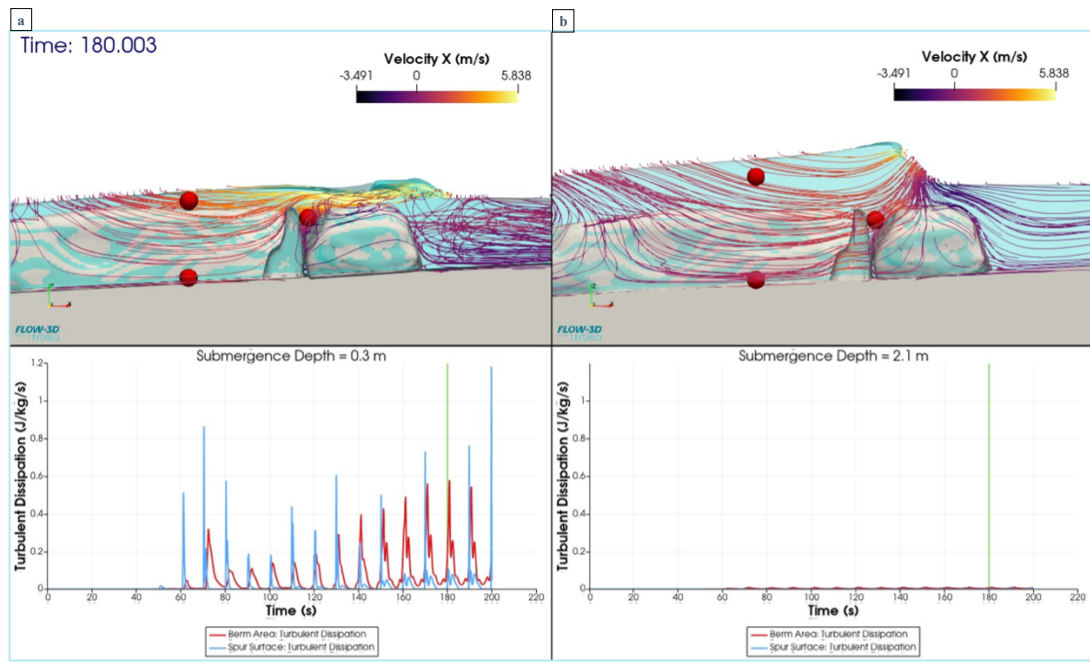
Figure 7. Wave breaking and turbulent dissipation changes in low tide and high tide conditions with the green line in the bottom plots indicating the time at which the upper images are shown. a. Groove cross-section during the low tide condition that correlated to a transmission coefficient of 0.56 where higher turbulent dissipation was observed in the berm area (red) and spur surface (blue). b. Groove cross-section during the high tide condition that correlated to a transmission coefficient of 0.73 where negligible values of turbulent dissipation were observed.

When evaluating wave height reduction as a function of submergence, a linearly decreasing trend was observed, Figure 8.

Figure 8. Plot showing the inverse relationship between wave height reduction and submergence.

The decrease in wave height reduction as the submergence increases correlates to the other trends observed with wave breaking and turbulent dissipation. Waves broke earlier on the structure in the low tide condition and much higher levels of turbulent dissipation were observed which likely contributed to the more significant wave height reduction. Since waves were transmitted past the structure in the high tide condition and virtually no turbulent dissipation occurred, the decline in wave height reduction was to be expected.

The changes in wave height reduction observed when varying wave period, groove width, spur length, and crest length were not significant in the testing indicating that the implemented model setup was not as sensitive to these parameters.

DISCUSSION

While the results did show certain wave height reduction trends during the sensitivity runs, it should be noted that the wave height reduction due to shoaling on the sloped bed was not subtracted from the overall reduction; therefore, these numbers do not reflect wave height reduction solely due to the artificial SAG reef breakwater. These results do, however, reflect typical hydrodynamic conditions in this configuration that would be more typical of the environment given the different flow responses from a sloped bed.

Larger waves induced stronger flows due to higher wave energy and also broke earlier due to depth limited breaking. Given the larger waves breaking earlier and in front of the crest, more reflection occurred and there was increased turbulence in the groove. The smaller wave saw an insignificant amount of turbulence due to no breaking over the structure. The trend of increased wave energy attenuation occurring as wave height increases follows typical patterns in conventional submerged breakwaters given that there is increased wave shoaling as wave height increases (Sharifahmadian 2015). By allowing smaller waves to be transmitted, normal circulation and sediment transport processes can occur which is beneficial for the overall coastal system. The effectiveness of the breakwater becomes more important as larger, erosive waves threaten the coastline.

While the wave height reduction did not show significant changes for varying wave period, the wave heights in front of the structure did vary due to different degrees of wave shoaling occurring. The wave height reduction due to the structure was between 35% and 40% for all periods tested, Table 4.

Table 4. Results for changes in wave period during the sensitivity run analysis.			
Wave Period (s)	Probe 2 Wave Height (m)	Final Wave Height (m)	Wave Height Reduction (%)
6	1.6	1	38
10	2.3	1.5	35
15	2.8	1.7	39

The shortest wave period appeared to have already decreased in wave height before the structure while the other simulations with greater wave periods steepened before the structure before breaking on the crest. Ultimately, the shortest wave period resulted in the smallest wave height.

Larger wave height reduction occurred in the lower submergence condition likely due to greater turbulence and frictional dissipation within the structure since the wave is forced to interact with the reef more than in the high tide condition. At the higher water level most of the waves are transmitted past the structure without interacting, and therefore yielding less energy attenuation.

Spur length was expected to increase wave height reduction as it increased since spurs in exposed to wave energy areas tend to be longer (Duce et al. 2016); however, insignificant changes were seen here likely due to increased submergence at the seaward end of the elongated spur. Future testing will maintain relative submergence across the entire length of the spur. Given the complexity and heterogeneity of a healthy coral reef, the simplification of the roughness height could also likely be contributing to an underestimate of shear stresses in the system. Since there is likely a relationship between the length of the spur and the wavelength of the incident wave, this aspect should be further studied, as well as testing with wider spurs to induce more wave reflection.

Increasing the crest length did not have significant effects on the wave height reduction or the flows; however, an important observation highlighting scour concerns was able to be made about the design of the structure. While making this reef as similar as possible to nature, it will never be exactly comparable to the system that a SAG and reef crest/flat zone create. Since the artificial SAG reef here is followed by sandy bottom and not a shallow, rocky reef flat, the waves tend to drop off after the crest as they break and create a large turbulence cell posing a risk for scour, Figure 9.
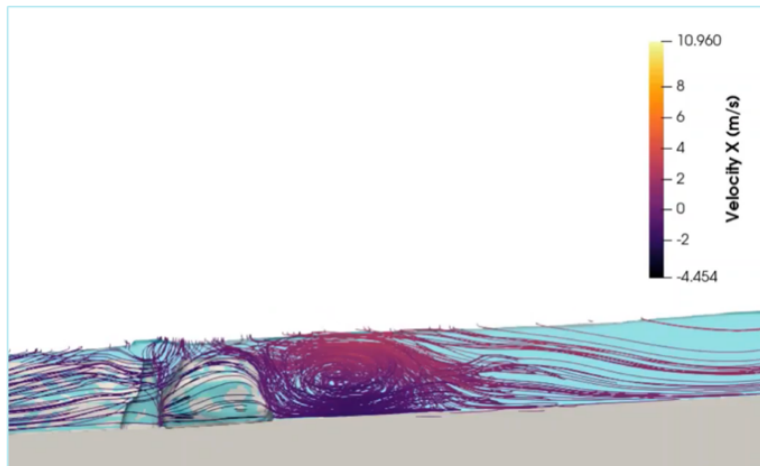
Figure 9. Evidence of potential scour from the formation of an eddy due to wave breaking in the lee of the structure.

Although sediment scour is not being studied here, the issue is evident. Because of the potential for scour, the crest module will be modified to have a sloping back in future iterations.

Groove width varies significantly worldwide but tends to be smaller in higher wave energy environments, so a small range of groove widths was tested. Insignificant changes in flow were found which agreed with findings in da Silva et al. (2020). From an engineering perspective these results prove to be beneficial since wider grooves require fewer materials, resulting in a reduction of costs for construction. Further testing will continue to widen the groove until a decline in wave height reduction is observed to find the maximum feasible groove width.

To reduce the overall number of simulations and streamline the testing process, each adjustment to the artificial SAG reef modules (i.e. changes in crest length, spur length, and groove width) were tested under the same wave and tidal condition; however, this research has not yet elucidated whether those changes to the structure would show more impacts to the hydrodynamics under variable conditions. Future studies will test sensitivity to structure dimensions under further variations of wave height, wave period, and depth due to tidal changes.

CONCLUSION

The model proposed in this study was sensitive to changes in wave height, wave period, and depth due to tidal changes. Although this work provides information into the initial design considerations of the structure, more research will need to be done to ensure optimal design. When designed incorrectly, any breakwater can result in negative impacts on the shoreline, including erosional hotspots, scour, and reduction of water quality. Future testing within the scope of this project will include incorporating crests with sloped backs, studying larger groove widths, testing multiple spurs and grooves, and finalizing a design for a storm wave. The sensitivity runs performed here aimed to select ranges that were deemed appropriate as a first step, but since there is no standard for design, much more extensive ranges likely need testing.

Future work outside of this project should focus on sediment transport effects, construction and installation procedures, thermal circulation, and wave tank testing on scale models for comparison to the simulations. Any artificial SAG reefs would need to be specifically designed for every subject site given that depth, wave conditions, and sediment transport processes can drastically vary from site to site. With appropriate design considerations, this project holds great potential for novel methods in green infrastructure and coastal resiliency.

While there is published research on the hydrodynamics on spur and groove reefs, only one paper thus far has modeled them in three dimensions and primarily focused on changes in circulation rather than the wave height attenuation capabilities of the reef (da Silva et al. 2020). Recent literature from Acevedo-Ramirez et al. (2021) showed that SAG structures have more impact in wave transformation than previously reported by other researchers given their findings of more than 99% wave energy flux dissipation during deployment in the Xahuayxol reef system. Since SAG reefs vary significantly

throughout the world and are found in energetic hydrodynamic conditions that make data collection difficult, there is a lack of data on these environments, and more research needs to be done to understand these systems.

Beyond the goal of simply attenuating waves like conventional breakwaters, this design promotes circulation that encourages the settlement of benthic flora and fauna and facilitates a healthy environment. A living breakwater helps decrease maintenance and the associated costs, while also promoting life in a new ecosystem. From the engineering perspective there are other benefits to using submerged breakwaters including their ability to let smaller waves pass, which allows normal cross-shore sediment transport processes to occur under mild conditions. Additionally, a submerged breakwater does not disrupt the aesthetics of the beach unlike emergent breakwaters, jetties, and groins. Green infrastructure and sustainable practices are important tools in the response to climate change at the global scale, and this project contributes research towards these aspects in the realm of coastal resiliency.

ACKNOWLEDGMENTS

REFERENCES

Acevedo-Ramirez, C. A., W. Stephenson, S. Wakes, and I. Mari.o-Tapia. 2021. Wave transformation on a fringing reef system with spur and groove structures. *Journal of Geophysical Research:Oceans*, 126, e2020JC016910.

Banks, K. W., B. M. Riegl, E. A. Shinn, W. E. Piller, and R. E. Dodge. 2007. Geomorphology of the southeast florida continental reef tract (Miami-Dade, Broward, and Palm Beach Counties, USA). *Coral Reefs*, 26(3), 617–633.

Campos, L., C. Castillo, and R. Molina-Sanchez. 2020. Damage in rubble mound breakwaters. Part I: historical review of damage models. *Journal of Marine Science and Engineering*, 8(5), 317.

da Silva, R. F., C. D. Storlazzi, J. S. Rogers, J. Reyns, and R. McCall. 2020. Modelling three-dimensional flow over spur-and-groove morphology. *Coral Reefs*, 39(6), 1841–1858.

Dattatri, J., H. Raman, and N. J. Shankar. 1978. Performance characteristics of submerged breakwaters, *Coastal Engineering Proceedings*, 1(16), 130.

Duce, S., A. Vila-Concejo, S. Hamylton, E. Bruce, and J. M. Webster. 2014. Spur and groove distribution, morphology and relationship to relative wave exposure, Southern Great Barrier Reef, Australia. *Journal of Coastal Research*, 70, 115–120.

Duce, S., A. Vila-Concejo, S. Hamylton, J. Webster, E. Bruce, and R. Beaman. 2016. A morphometric assessment and classification of coral reef spur and groove morphology, *Geomorphology*, 265, 68–83.

Duce, S., A. Vila-Concejo, R. McCarroll, B. Yiu, L. Perris, and J. Webster. 2022. Field measurements show rough fore reefs with spurs and grooves can dissipate more wave energy than the reef crest, *Geomorphology*, 413, 108365.

Eddy, T. D., V. W. Lam, G. Reygondeau, A. M. Cisneros-Montemayor, K. Greer, M. L. D. Palomares, J. F. Bruno, Y. Ota, and W. W. Cheung. 2021. Global decline in capacity of coral reefs to provide ecosystem services. *One Earth*, 4(9), 1278–1285.

Florida Institute of Oceanography (FIO). 2021. Consortium for advanced reef restoration, engineering and technologies (CARRET) proposal.

Flow Science, Inc. 2008. FLOW-3D® Version 9.3 User Manual.

Gittman, R. K., S. B. Scyphers, C. S. Smith, I. P. Neylan, and J. H. Grabowski. 2016. Ecological consequences of shoreline hardening: a meta-analysis. *BioScience*, 66(9), 763–773.

Google Maps. n.d.. Google Maps.

Irtem, E., E. Seyfioglu, and S. Kabdasli. 2011. Experimental investigation on the effects of submerged breakwaters on tsunami run-up height. *Journal of Coastal Research*, 64, 516–520.

Kobayashi, N., and A. Wurjanto. 1989. Wave transmission over submerged breakwaters. *Journal of Waterway, Port, Coastal, and Ocean Engineering*, 115(5), 662–680.

Lowe, R. J., J. L. Falter, S. G. Monismith, and M. J. Atkinson. 2009. Wave-driven circulation of a coastal reef–lagoon system, *Journal of Physical Oceanography*, 39(4), 873–893.

Masselink, G., B. Castelle, T. Scott, G. Dodet, S. Suanez, D. Jackson, and F. Floc'h. 2016. Extreme wave activity during 2013/2014 winter and morphological impacts along the Atlantic coast of Europe. *Geophysical Research Letters*, 43(5), 2135–2143.

Munk, W. H., and M. C. Sargent. 1948. Adjustment of Bikini Atoll to ocean waves. *Transactions, American Geophysical Union*, 29(6), 855.

Ogston, A., C. Storlazzi, M. Field, and M. Presto. 2004. Sediment resuspension and transport patterns on a fringing reef flat, Molokai, Hawaii, *Coral Reefs*.

Rogers, J. S., S. G. Monismith, F. Feddersen, and C. D. Storlazzi. 2013. Hydrodynamics of spur and groove formations on a coral reef, *Journal of Geophysical Research: Oceans*, 118(6), 3059–3073.

Sharifahmadian, A. 2015. *Numerical Models for Submerged Breakwaters: Coastal Hydrodynamics and Morphodynamics*. Elsevier Gezondheidszorg.

Storlazzi, C., A. Ogston, M. Bothner, M. Field, and M. Presto. 2004. Wave- and tidally-driven flow and sediment flux across a fringing coral reef: Southern Molokai, Hawaii, *Continental Shelf Research*, 24(12), 1397–1419.

United States. 2006. Coastal engineering manual – part V. Washington, D.C.: U.S. Army Corps of Engineers.

Vousdoukas, M. I., R. Ranasinghe, L. Mentaschi, T. A. Plomaritis, P. Athanasiou, A. Luijendijk, and L. Feyen. 2020. Sandy coastlines under threat of erosion. *Nature Climate Change*, 10(3), 260–263.

Wood, R., and C. Oppenheimer. 2000. Spur and groove morphology from a Late Devonian reef. *Sedimentary Geology*, 133(3–4), 185–193.

Yakhot, V., and S. A. Orszag. 1986. Renormalization group analysis of turbulence. I. Basic theory. *Journal of Scientific Computing*, 1(1), 3–51.